Three-dimensional, Broadband Seismometer Array Experiment at the Homestake Mine

V. Mandic[a], V.C. Tsai[b], G. Pavlis[c], T. Prestegard[a], J. Atterholt[c], D.C. Bowden[b], P. Meyers[a], R. Caton[c]

[a] School of Physics and Astronomy, University of Minnesota, Minneapolis, MN 55455, USA
[b] California Institute of Technology
[c] Indiana University

Introduction

Seismology has been a ubiquitous tool for determining subsurface Earth structure and learning about various dynamic sources, including earthquakes and nuclear explosions [standard seismology REF]. The number of seismic arrays has grown appreciably in the last few decades, with over 7000 broadband seismometers deployed within the United States alone, and over 20,000 worldwide [iris REF]. However, despite this large number of seismometers, instruments have largely been confined to the Earth's surface, with few stations having been placed at depths greater than 100 meters, primarily due to the obvious practical difficulty of getting to such depths. The few exceptions include seismometer arrays within single boreholes (TCDP, Parkfield REF) and in active mines (S. Africa and other REF), and frequently such instruments have been limited to high-frequency geophones rather than more broadband seismometers [REF].

While observing ground motions at or near the Earth's surface has generally been acceptable, there are a number of reasons why observations at deeper depths, particularly from an array of instruments, would potentially be useful. First and foremost, it is well known that most seismic 'noise' is generated near the surface [noise REF] and that this noise generally decreases significantly with depth [borehole REF]. Observations at depth therefore have the potential to be less contaminated by surficial noise, and therefore may more accurately measure the elastic waves arriving from geophysical sources of interest. The second main reason that seismic measurements at depth could be advantageous is that Earth structure generally decreases in complexity with depth, with most of the highly weathered and sedimentary deposits being confined near the surface [REF]. Not only do such features typically cause much slower velocities, but they cause the Earth to be highly heterogeneous and strongly scattering, resulting in complexity of wave propagation that is challenging to model and interpret. Since nearly all observations contain this complexity, it is not known precisely how severe the effect is, but it is expected that observations far away from such heterogeneities are simpler and more predictable.

In addition to illuminating fundamental questions on seismic wave propagation, seismic measurements at depth are also of interest in the field of gravitational wave astrophysics. The Laser Interferometer Gravitational-wave Observatory (LIGO) recently announced

the first direct detections of gravitational waves produced in a merger of binary black hole systems [LIGO REFs], hence ushering a new field of inquiry in astrophysics. To fully explore the scientific potential of this field, more sensitive detectors are needed, and are in process of being designed [ET, CE REFs]. One of the limiting noise factors in these detectors at frequencies below 10 Hz is the seismic noise that causes fluctuations in the local gravitational field. It is expected that this noise source will be reduced underground due to the suppression of surface seismic waves, but it is currently not understood what is the sufficient depth for these detectors, nor what is their optimal configuration. Underground seismic measurements are therefore needed to quantify these effects, thereby directly informing the design of the future generations of gravitational wave detectors.

To explore the promise of subsurface seismological observations, both for geophysical and astrophysical applications, we have built and operated an underground three-dimensional (3D) array at the Homestake Mine in Lead, SD, which was one of the largest and deepest gold mines in North America; we report on this unique 3D array in this publication. The Homestake Mine officially closed operations in 2002, but reopened in 2007 as the Sanford Underground Research Facility (SURF), and currently features several other experiments, including dark matter and neutrino experiments that benefit from the cosmic ray shielding of the rock overburden. The significant infrastructure in the Homestake Mine, including easy access to numerous underground levels with hundreds of km of available drifts, availability of power and network, and safety protocols and infrastructure make the Homestake Mine an ideal location for the development of a 3D seismometer array.

In this paper, we describe the novelty of the 3D Homestake array as compared to other subsurface seismological deployments, the experience learned in operating the underground array for 2 years, and preliminary results that demonstrate the potential that such data have. While the results described here are not expected to be the final products of the Homestake array, we anticipate the results to be useful both for future experiments of a similar type and as a foundation for later analysis.

Seismometer Array

The Homestake seismometer array consisted of 24 seismic stations, 15 underground and 9 on the surface, depicted in Figure 1. The locations of stations are known with uncertainties on the order of 2 m. Underground station locations were obtained from maps of the mine drifts based on past mine surveys, while surface station coordinates come from GPS data. All of the underground stations were installed between December 2014 and March 2015, and remained operational until December 2016. The surface stations were installed in May 2015 and remained operational until September 2016. The seismic equipment used in the experiment was provided by the Portable Array Seismic Studies of the Continental Lithosphere (PASSCAL) instrument center, which is a part of the Incorporated Research Institutions for Seismology (IRIS). Most stations used a Streckheisen STS-2 high-sensitivity broadband seismometer. The exceptions were the underground station 300 and three surface stations, where we deployed the more water resistant Guralp CMG-3T seismometers.

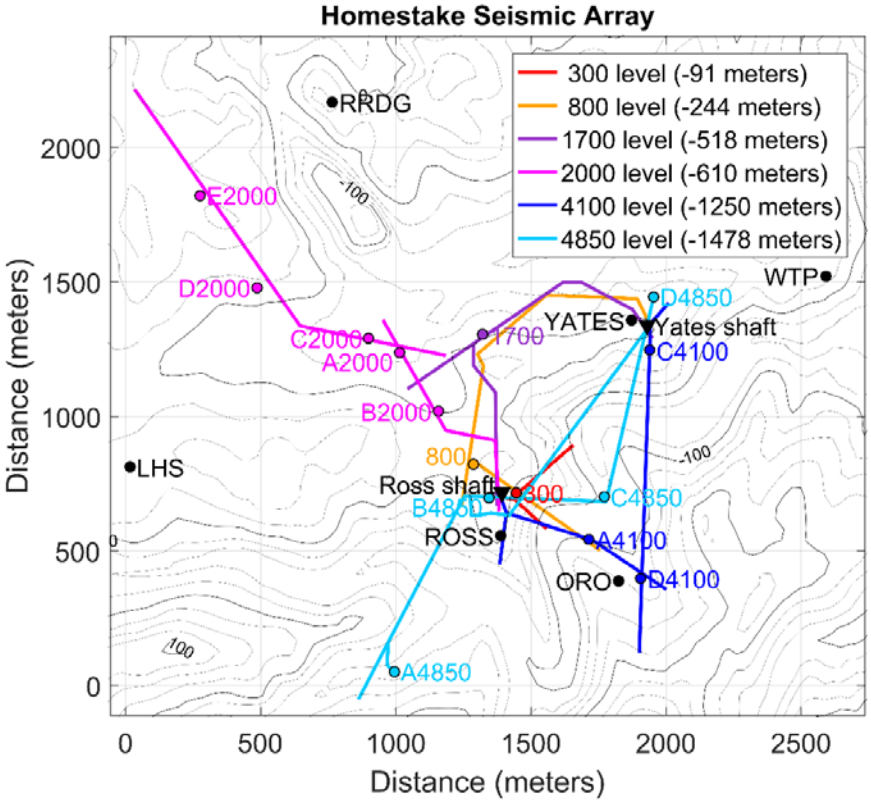

Figure 1: Homestake seismometer array layout. The lines of different colors depict the relevant drifts at various depths, along which we installed underground seismic stations. The black filled circles denote the surface stations (remote surface stations DEAD, SHL, and TPK were located outside the depicted region). Also shown are the two shafts at the Homestake mine, known as the Yates and Ross shafts, denoted by black filled triangles.

The underground stations were scattered across several levels: one at the depth of 300ft (91 m), one at 800 ft (244 m), one at 1700 ft (518 m), five at 2000 ft (610 m), three at 4100 ft (1250 m), and four at 4850 ft (1478 m). The locations of these stations were chosen to maximize the horizontal aperture of the array within the constraints imposed by safe access, availability of power, and access to SURF's fiber optic network. In several cases we had to extend existing power and network cables to support the stations. We strove to locate sites as far as possible from activity in the mine and from water drainage pathways. Stations were usually placed in alcoves or blind alleys to minimize the effects of the air drifts, although several stations were installed in enlarged areas within the main drifts of the mine. In most cases, we found there were complex tradeoffs between cost of installation and distance from active operations.

Many sites had existing concrete pads of various sizes and thicknesses from the original mine operation. When necessary we poured a concrete pad directly onto the rock. In all cases a granite tile was attached to the pad using thinset mortar. All underground site preparation was completed three (or more) months prior to the installation of the instruments. Each seismometer was placed directly onto the granite tile, and was oriented to cardinal directions using an Octans gyrocompass from the IRIS-PASSCAL instrument center. To reduce acoustic noise induced by air flow we covered each sensor with two nested huts constructed of 2" thick polyisocyanurate foam panels and sealed with foam sealant. The digitzer was placed several meters away, and

included a Q330 data logger, a baler, and network and power supply electronics. Each station was powered by a small 12V battery continuously charged by a simple AC charger. The battery provided approximately a one day power reserve, which proved more than adequate to cover any power outages encountered during the experiment.

In addition to saving the data locally with a baler, we utilized real-time telemetry for all underground sites and six of the nine surface sites. The underground stations were synchronized using a custom-designed GPS optical distribution system. The GPS signal was received by a GPS antenna mounted on the roof of the SURF administration building and piped to a Q330 in the server room of the same building. This "master" Q330 data-logger was used to convert the received high-frequency GPS signal into the separate 1PPS (1 pulse-per-second) and NMEA metadata components that were used as an external timing signal for the underground instruments. The output from the master Q330's EXT GPS port was fed into an electro-optical transceiver to convert the analog voltage output to optical signals. The transceivers were custom-made for this application by Liteway, Inc. (model number GPSX-1001). An optical-fiber network of optical splitters and transceivers was installed underground to distribute this GPS timing signal to all underground stations, while maintaining its signal-to-noise ratio throughout the mine. At each station, a transceiver was used to convert the optical signals back to electrical, which were then sent into the Q330's EXT GPS port. Phase errors logged by the Q330 digitizers suggest the timing precision achieved with this system was of the order of 1 μs. Systematic errors from propagation and electronic delays were negligible.

Five of the nine surface stations were located on SURF property above the underground stations. Another station was located at Lead High School (LHS) in collaboration with the Lead Deadwood Public School District. We deployed the remaining three stations on private land in an outer ring at a nominal radius of 5 km from the array center. We used conventional, portable broadband sensor vaults but carefully separating the wall of the sensor vault from the concrete pad poured at the bottom. This detail is known from early experience in the 1990s at IRIS-PASSCAL to reduce tilt noise from soil motions. All but one of the sites (DEAD) were bedrock sites with a concrete pad poured on weathered metamorphic rocks of variable lithologies. The surface stations were all oriented by conventional compass methods, which means the precision is less than the underground sites oriented with the Octans instrument. We insulated the sensor vault with a layer of foam and burial with as much of a soil cover as possible. We had the common problem of rain washing some cover away that we restored when the instruments were serviced.

While the three outer stations were stand-alone, the remaining six inner stations all used radio telemetry. Of these, the LHS site located near a high-school used a point-to-point radio that linked the outdoor site to a Linux computer in a computer laboratory at the school. The remaining five stations were radio-linked to a master radio on the roof of the SURF administration building where our data logging computer was located. All surface sites except LHS used solar power; LHS used an AC system similar to underground sites but with a larger battery backup. All surface sites used the standard Q330 GPS timing system.

The telemetry system we deployed used a computer running the Antelope software at the SURF administration building to handle real time communication to all underground sites and five of the nine surface sites. We ran a separate Linux computer running Antelope at LHS to handle real time communications with that single site. This approach was necessary to deal with firewall issues at both SURF and the high-school. We then set up an orb2orb feed to a University of Minnesota computer that acted as a data concentrator. The participating institutions and the IRIS-DMC were then able to tap that connection for real-time feeds with a latency of a few tens

of seconds. We developed a custom monitoring system to automatically test for a range of conditions and build web-based quality control summaries. We also set up a rotating shift schedule to monitor this diagnostic information on daily basis. This allowed us to quickly identify and diagnose problems. This was a major factor in the exceptionally high data recovery rate of this experiment (near 100% for every site except DEAD, which had power problems in the winter of 2015-2016). Furthermore, the telemetry data have no mass position related issues except for two sensors failures. In addition, this quality control monitoring allowed us to detect and diagnose a subtle problem on station E2000. That station began showing odd tilt transients, which site visits revealed was created by a failure of the thinset grout on the base of one of our granite tiles. This was repaired by pouring a new concrete pad and setting the tile directly on the concrete.

Preliminary Results

Noise Spectra

The ambient seismic noise levels at the Homestake mine, especially at the deepest levels, are remarkably low and stable. We demonstrate this by computing the displacement amplitude spectral density (ASD) of seismic noise over long periods, for different stations and for different seismic channels (east, north, vertical). We use one year of data (from June 1, 2015–May 31, 2016), split into 400 second intervals. The median amplitudes in each frequency bin for the vertical seismic channel are shown in Figure 2 in comparison to the low- and high-noise models by Peterson [REF]. The left panel compares the ASDs for stations at several different depths. All of the stations are in close agreement in the middle range of frequencies, which corresponds to the microseismic peak. At higher frequencies, there is significantly less noise with depth: above 0.5 Hz, the stations at 4100 ft and 4850 ft depths are nearly an order of magnitude quieter than other stations. At the lowest frequencies there is also a good agreement between the stations, although a slight increase in noise is apparent in the surface stations; this may be due to larger temperature variations closer to the surface inducing tilts in the concrete pads. While the underground stations at any given depth tend to agree very well, there is a wide range of variability among the surface stations, as depicted in the right panel of Figure 2. This is due to differences in the local environment in terms of thermal insulation and proximity to human activity.

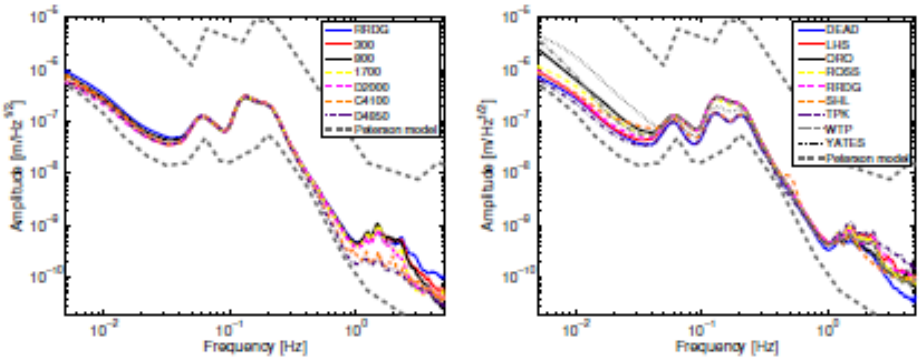

Figure 2: Median amplitude spectral densities for Homestake seismic stations. Numbered legend entries denote depth in feet, while numberless legend entries denote surface stations. Peterson low- and high-noise models are shown as dashed gray lines. See text for more detail.

Figure 3 shows ASD histograms for the RRDG surface station (left) and for the A4850 underground station (right) as examples of a relatively good surface station and our deepest and

most isolated underground station. Here, we show histograms of ASDs calculated from the 400-second data intervals over 1 year in each frequency bin, revealing the overall variability of the seismic noise at each station. The white curve represents the median ASD (identical to those shown in Figure 2), the black curves represent the 95% confidence intervals in each frequency bin, and the color scale shows the overall distribution. The Peterson low- and high-noise models are shown in dashed gray.

The histograms display about two orders of magnitude of variation across all frequencies for both the RRDG station and the A4850 station. The A4850 station measures less noise in general and appears to have less overall variation than RRDG. There also appears to be significantly more high-frequency noise in the RRDG station; this is likely due to anthropogenic surface waves that are suppressed with depth. Both stations stay within the low- and high-noise Peterson models most of the time. However, in the 0.3–0.9 Hz range the A4850 station is actually below the low-noise model a significant fraction of the time. We also observe a considerable difference between the vertical channel and the horizontal channels at low frequencies: at 0.01 Hz and below for both stations, the vertical channel has almost an order of magnitude lower noise than the horizontals, likely caused by the slow tilting of the ground.

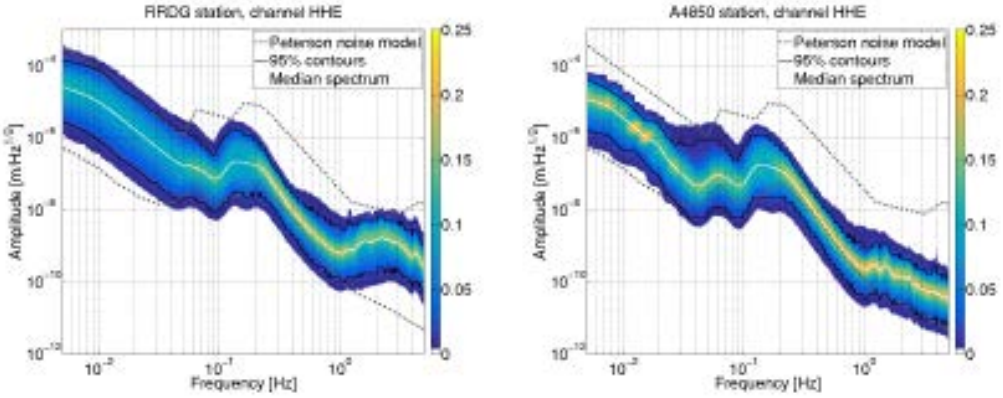

Figure 3: Histograms of amplitude spectral density in each frequency bin for a surface station (left) and for an underground station at 4850 ft depth (right). Median ASDs (solid white), 95% confidence intervals for each frequency bin (solid black), and the Peterson low- and high-noise models (dashed gray) are shown. See text for more details.

Array Analysis of Event Data

To date we have processed six months of data to identify seismic events. This has required a mix of conventional and unconventional analysis. A technical problem we faced is that this array was located in an area with some of the sparsest coverage in the country. In an area with sparse coverage, an array of 24 ultra quiet sites dominates detection limits and violates implicit assumptions of conventional automated detectors. Figure 4 shows the 8 regional stations we used to detect and locate local and regional events. We used the automated detectors and location system in the Antelope 5.6 (http:://brtt.com latest access April 25, 2017). When we used all channels from the array in combination with the sparse regional coverage we had a large number of spurious detections. Although some are definitely local sources and might be of interest in other studies, our initial interest was in the events with the best signal-to-noise ratio where the plane wave approximation was valid for phased array processing. We reduced the false

detection rate to near zero by running the detection algorithm only on the three outer surface sites (DEAD, TPK, and SHL) and one of the quietest underground sites (D4850), and by requiring six P-wave associations before declaring an event.

The most significant impact of this choice is that we dropped all of the events from the local mine with example seismograms shown in Figure 5. The source for those seismograms is without doubt an active surface mine whose boundary is only 2.5 km west of station TPK. Figure 4 is thus incomplete, as it does not show any events from this potentially useful data source. Review of data from initial detector runs that detected these events indicates that this mine blasts at least once per day during the workweek. There are thus a large number of seismograms like Figure 5 that could be used in future studies, for example of wave propagation at high frequencies. Note that this Figure clearly shows the theoretically expected suppression of the Rayleigh wave with depth. With the true amplitude scaling of Figure 5, the Rayleigh wave is barely visible on any of the stations in the 4000s subarray.

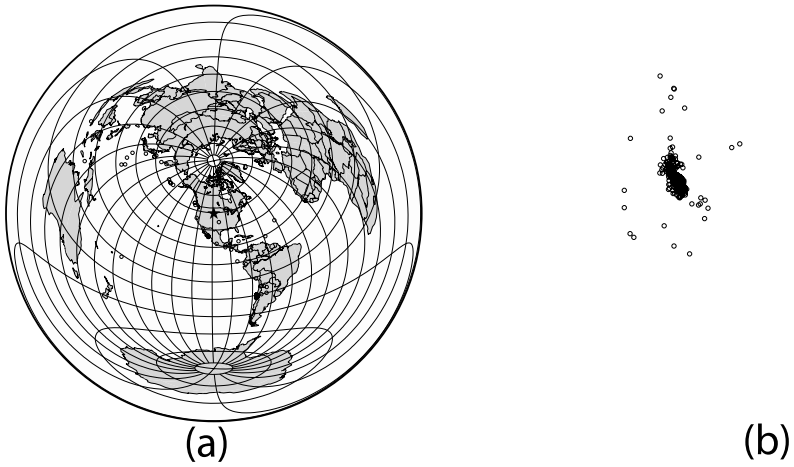

Figure 4. Epicenter maps of events recorded by Homestake 3D array. (a) An azimuthal equal distance projection map centered at the array site marked with a star. Epicenters of distant earthquakes recorded by the array in the 2015 study period are shown as circles. (b) Epicenter map focused on local and regional events. The array location is again shown as a star and estimated event epicenters are shown as circles. Black filled triangles are regional stations used for detection and location of the events plotted.

We used a standard analyst review method to produce the epicenter maps shown in Figure 4. Of 431 epicenters, 359 are in the local area shown in the right panel of Figure 4 and 72 are at regional to teleseismic distances shown in the left panel of Figure 4. The locations shown were produced by association with epicenter estimates produced by U.S. Geological Survey catalogs and assembled at the USArray Array Network Facility (http://anf.ucsd.edu/events/ last access April 27, 2017). We estimated the local event epicenters shown in Figure 4 (right) with the dbgenloc program [REF] using the IASP91 earth model using travel time picks made by standard, interactive analyst review methods. Every one of 359 events shown in Figure 4 (right) are almost certainly mining explosions from coal mining in the Powder River Basin. All have similar waveforms with emergent P waves and prominent surface waves like the event shown in Figure 5.

We assumed this was the case and fixed the depth of all these events for the location estimates used for Figure 4 (right). Most of the events cluster in the area of the coal mining district. There are some outliers that are almost certainly poorly constrained epicenter estimates that have been badly mislocated. These events are characterized by picks at only one regional station in addition to the array, which creates a poor constellation for location.

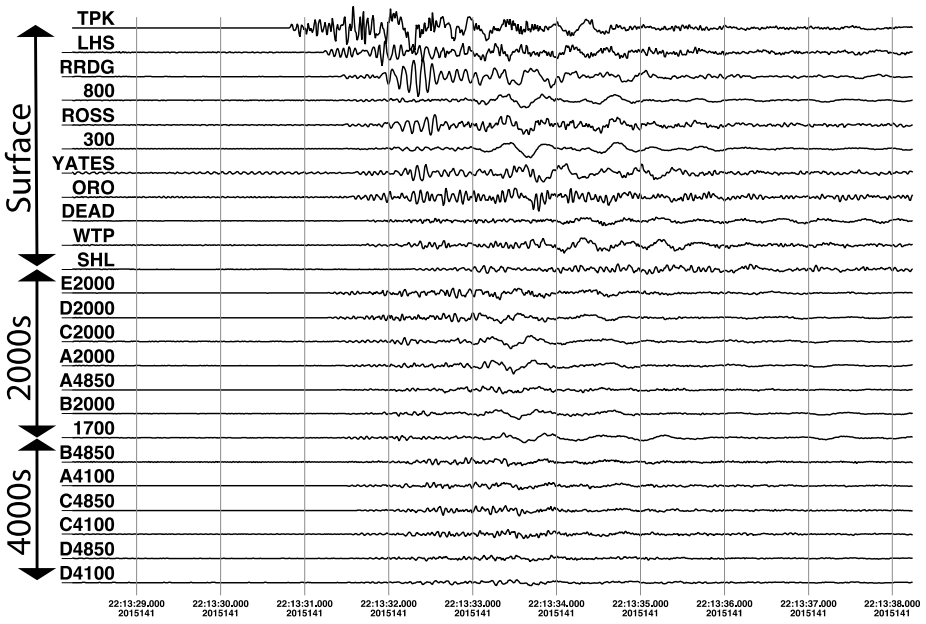

Figure 5. Vertical component seismograms from local surface mine. Seismograms are displayed at true amplitude and grouped by subarrays used throughout this paper. Records for each subarray are sorted by epicentral distance from the estimated source location (approximately 4 km west of TPK). Subarrays are ordered by increasing depth. [VM: WHY IS A4850 INCLUDED IN 2000s SUBARRAY?]

This problem is solvable by using an array slowness vector estimate by plane wave processing like that described below, but at the time of submission we had not completed that processing. Most, if not all, of the scattered epicenters in Figure 4 (right) are likely explosions from Powder River Basin coal mines. [VM: DO WE NEED THIS PARAGRAPH? MAYBE DELETE OR ADD A SHORT SENTENCE AT THE END OF LAST PARAGRAPH?]

We processed all the events with locations shown in Figure 4 with a nonstandard array processing method. When we examined waveforms recorded by the array it was immediately clear that simple delay and sum phased array processing was problematic. Notice that the broadband P waveforms seen in Figure 6 (a and b) are very well matched for this large event for only the first cycle of the P wave. When the same data are filtered to short periods there are very large variations in the waveforms at distance scales that are a fraction of the wavelength of P or S body waves. Although not shown, surface and underground waveforms in the short period band are commonly wildly different. Figure 7 shows this problem is even more dramatic for typical coal mine explosions from

Wyoming (Figure 4 (right)). Note the very strong changes in amplitude and waveform shape for subarray stacks from different levels in mine.

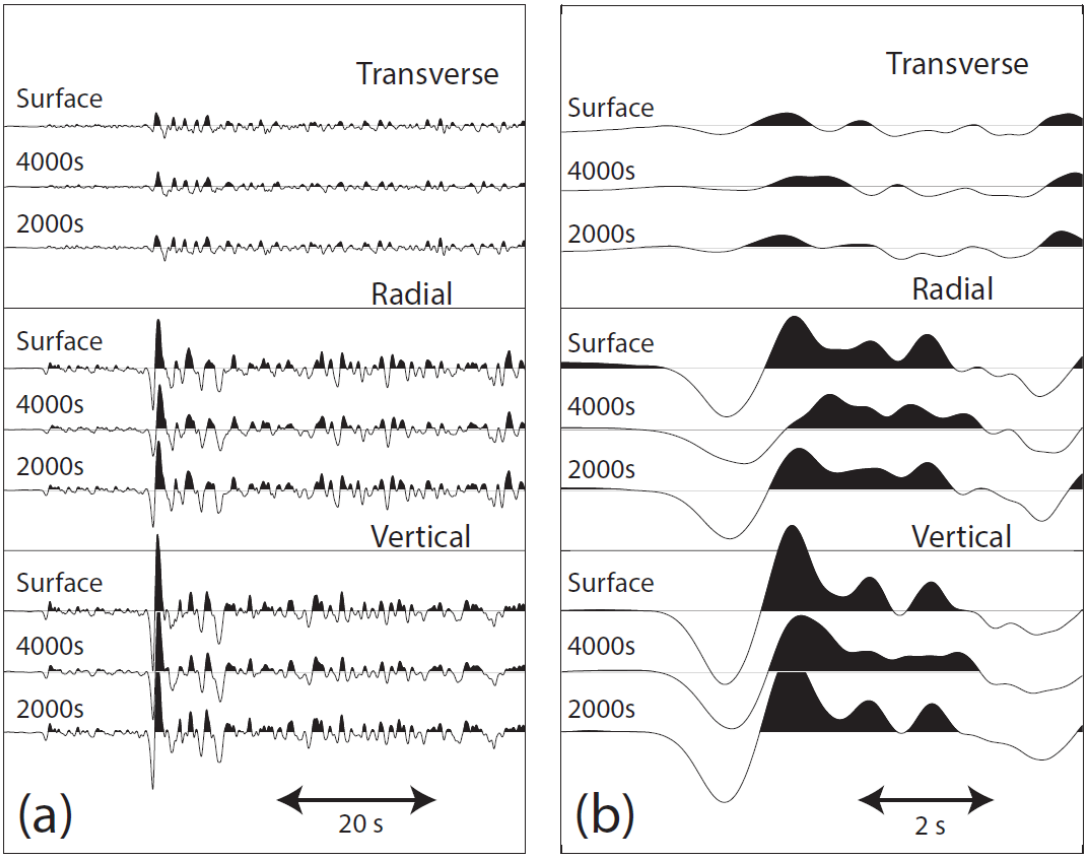

Figure 6: Alaska earthquake records from Homestake 3D array. (a) illustrates the three components of subarray stacks defined in the text. (a) shows the first 2 minutes of the data following the P wave signal. These data were filtered with a 0.01 to 2 Hz bandpass filter before stacking. The P wave of this event is much smaller than the pP phase seen approximately 25 s after P (event depth is 120 km and distance is 33°). (b) shows a shorter time window focused on only the P wave (6 s following measured P time). All plots are true amplitude meaning amplitudes differences between seismograms are real. In all figures the seismograms have been aligned by cross correlation before stacking. Stacks are aligned manually.

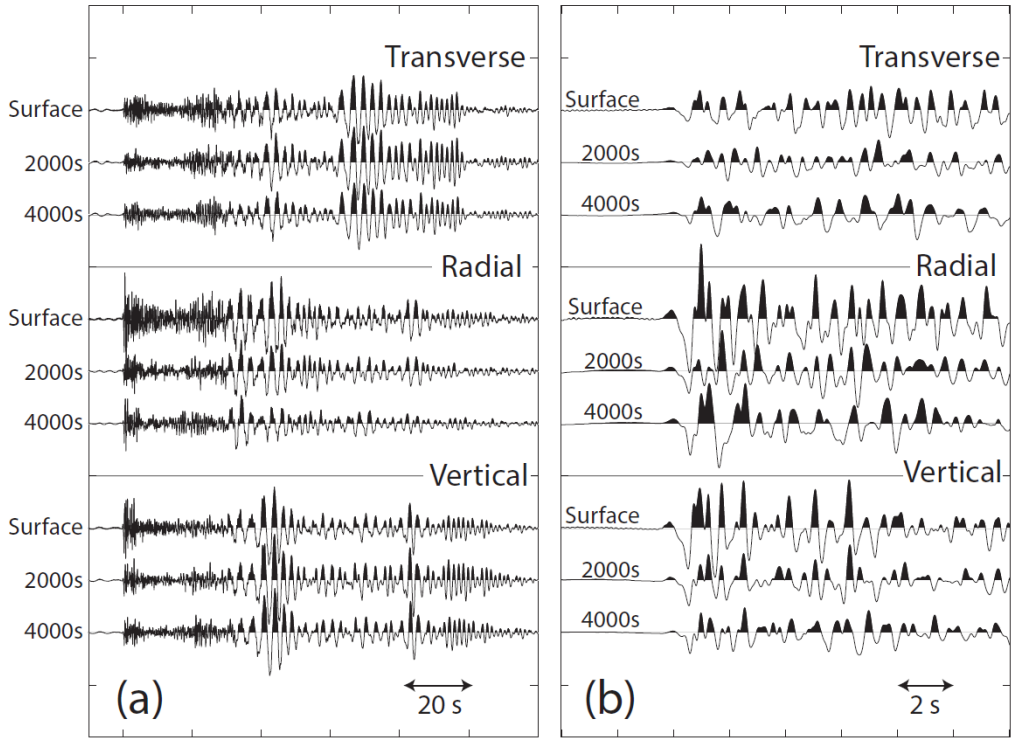

Figure 7: Seismograms from a typical Powder River Basin coal mining explosion recorded by the Homestake 3D array. All the data shown in this figure were filtered with a 5 pole Butterworth filter with a pass band from 0.25 to 10 Hz. (a) shows 2 minutes of data following P-wave and is directly comparable to Figure 6a. (b) is directly comparable to the Figure 6b but for this explosion source instead of a teleseismic earthquake. (b) shows subarray stacks for 6 s of data following the measured P wave time. We show the 2000s subarray here because for this event that subarray is oriented roughly in the direction of propagation of the P-wave. All figures show seismograms in true amplitude and seismograms were again aligned by a mix of cross-correlation and manual picks.

Because of the depth dependence of waveforms we processed each of the 3 subarrays shown in Figure 5 with a program called dbxcor (Pavlis et al., 20??) in a subarray mode. dbxcor does not use a plane wave approximation, but computes lags relative to a stack estimated by a robust method described by Pavlis et al. (201??). While it was originally designed for large aperture arrays like the USArray, we found it worked well in this setting. Note, however, that in dbxcor processing the cross-correlation window was always much shorter than shown in these figures and defined interactively by the analyst. Typical correlation window sizes were 2-4 s for the local mining blasts and 10-20 s for teleseismic events. We have found no unbiased way to correlate subarray stacks to more precisely measure time delays between subarrays. Consequently, at present we have only used manual picking to align subarrays as shown in these figures.

Figures 6 and 7 show the three-components of the stack of the aligned seismograms from each subarray. Figure 7 shows clear evidence for a depth dependence in amplitudes for

the mining explosions. Furthermore, the variation in the P-wave waveforms in Figure 6 is suggestive of the P to surface wave scattering in the teleseismic event. For the nominal period of 1 s for these data, the wavelength for P-wave is about 6 km and for S-wave is about 3.5 km. Figure 6, however, shows large variations in waveforms over distances of the order of 200-300m which are difficult to explain with some type of scattering. [GARY TO EXPAND ON THIS]

Conclusions (TBD, let's see what the paper looks like)

We have described a three-dimensional array of high-sensitivity broadband seismometers in the Homestake mine, SD, spanning roughly a cubic mile underground. We have also shown preliminary results of analyses of data acquired by this array. The data are characterized by exceptionally low seismic noise levels that are also very stable over a year-long time scale. Consequently, the data offer a wide range of possible studies to better understand wave propagation. The data contains high signal-to-noise records of hundreds of transient signals, both due to local or regional mining blasts and due to teleseismic events. The preliminary look at these transient events reveals rich structure in terms of depth dependence of different wave components, and in terms of interaction of waves with the surface.

Several studies are underway examining some of these effects in further detail. The transient events offer multiple ways to estimate the seismic wave speed, both locally in the Homestake mine, and in the region. The depth dependence of waveforms in these transients is also used to determine the depth eigenfunctions for Rayleigh and Love waves. This information will be combined with radiometer-based techniques used in other areas of physics to attempt estimates of directionality and modal composition of the ambient seismic noise. Such estimates would directly contribute to the design of future underground gravitational-wave detectors. The depth and temporal dependence of teleseismic events is also being used to understand the scattering and reflection of the nearly-vertical incoming waves with the surface, hence directly measuring the impact of the surface weathered layer on the teleseismic waveforms. Finally, active excitation experiments were conducted, with excitations performed both on the surface and underground, providing additional information on wave propagation, reflections, and scattering. These studies will be subjects of future publications.

References

Some topics not necessarily addressed in the introduction:
- Review of literature on applied geophysics underground measurements – this is a simple search in Geophysics. A LOT has been done for the mining industry and we need a perspective
- Basic geology review – note the rocks are schists and phyllites and high precision mapping data is preserved at Sanford lab

THE FOLLOWING IS RELATED TO THE SLOWNESS FIGURE WHICH WE DECIDED NOT TO INCLUDE:

The cross-correlation method we used produced arrival time estimates for each array station processed. For the events plotted in Figure 4 a plane wave approximation is reasonable. For a plane wave the arrival time at station *i*, T_i, relative to the arrival time T_0 at a reference point is

(1) $$T_i = T_0 + \boldsymbol{u} \cdot \boldsymbol{\Delta x}_i$$

where $\boldsymbol{u}$ is the three-dimensional slowness vector defining the plane wave and $\boldsymbol{\Delta x}_i = \boldsymbol{x}_i - \boldsymbol{x}_0$ is the offset vector between station *i* and the reference point, $\boldsymbol{x}_0$. This is the standard moveout equation for plane-wave array processing, but in every seismic array we are aware of the z-component was not resolvable. Equation 1 defines a linear inverse problem with arrival times as the data and four unknowns: $T_0, u_x, u_y,$ and u_z. We initially tried a simple least-squares fit to arrival times measured by dbxcor, but we found this produced very unreliable estimates of u_z. We found this was caused by inconsistencies in hand picks of the array stack arrival time between subarrays. To address this we did a simple grid search with two parameters, $\Delta\tau_{surface}$ and $\Delta\tau_{4000s}$, that define time shifts applied to all data from the surface and 4000s subarray respectively (see Figure 5 for station definitions). For each assumed time shift we solve Equation 1 by least squares. We use the solution with smallest (L2 norm) residual as our best estimate of the slowness vector and T_0.

Figure 8 summarizes the results of applying this algorithm to all the events plotted in figure 4. The results for the Wyoming mine event are clustered at an azimuth and slowness consistent with the comparable cluster of event seen in Figure 4. There are a number of outliers that with these data alone would appear to come from outside the Powder River Basin area. However, those outliers do correspond to epicenters in Figure 4 we argued earlier were mislocated. Instead the are almost certainly errors in the slowness vector estimates that are most likely due to cycle skips in the cross-correlation analysis with dbxcor that were not caught by the analyst. In contrast, the teleseismic

event slowness vectors are all consistent with the back azimuth expected from the catalog locations (CROSS CHECK THIS ASSERTION).

Discuss total slowness magnitude and statics issue.

Figure SLOWNESS. Slowness estimates for all events plotted in Figure EVENTMAP. All three parts of the figure plot the x and y components of the slowness vector estimates as independent variables with a circle symbols at the estimated position for the two horizontal components. The circle are drawn on the figures to illustrate constant horizontal slowness vector magnitude ($\sqrt{u_x^2 + u_y^2}$). Parts (a) and (c) color code the slowness estimate by the estimated vertical component. (b) parameterizes the relative size of the vertical and horizontal components in a different way by the inclination angle $\theta = \tan^{-1}\left(u_z/\sqrt{u_x^2 + u_y^2}\right)$. Parts (a) and (b) show results for events less the 2.5° from the array while (c) shows results for event greater more than 2.5° from the array.